Identification of Higher Order Long-Propagation-Length Surface Plasmon Polariton Modes in Chemically Prepared Gold Nanowires

Aniruddha Paul,[†] David Solis, Jr.,[‡] Kui Bao,[§] Wei-Shun Chang,[†] Scott Nauert,[†] Leonid Vidgerman,[†] Eugene R. Zubarev,[†] Peter Nordlander,[§,‡] and Stephan Link[†,‡,*]

[†]Department of Chemistry, [‡]Department of Electrical and Computer Engineering, and [§]Department of Physics and Astronomy, Laboratory for Nanophotonics, Rice University, Houston, Texas 77005, United States

ABSTRACT A comprehensive understanding of the type of modes and their propagation length for surface plasmon polaritons (SPPs) in gold nanowires is essential for potential applications of these materials as nanoscale optical waveguides. We have studied chemically synthesized single gold nanowires by a novel technique called bleach-imaged plasmon propagation (BIIPP), which relies on the plasmonic near-field induced photobleaching of a dye to report the SPP propagation in nanowires. We observed a much longer propagation length of $7.5 \pm 2.0\ \mu$m at 785 nm compared to earlier reports, which found propagation lengths of $\sim 2.5\ \mu$m. Finite difference time domain simulations revealed that the bleach-imaged SPP is a higher order $m = 1$ mode and that the lowest order $m = 0$ mode is strongly quenched due to the loss to the dye layer and cannot be resolved by BIIPP. A comparative assessment of BIIPP with direct fluorescence imaging furthermore showed that the significant difference in propagation lengths obtained by these two techniques can be attributed to the difference in their experimental conditions, especially to the difference in thickness of the dye layer coating on the nanowire. In addition to identifying a higher order SPP mode with long propagation length, our study infers that caution must be taken in selecting indirect measurement techniques for probing SPP propagation in nanoscale metallic waveguides.

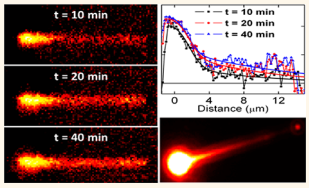

KEYWORDS: gold nanowires · surface plasmon polaritons · plasmon propagation · plasmonic waveguides · fluorescence imaging

The miniaturization of optical elements is critically important for the further development of photonic and optoelectronic devices.[1−6] A major challenge is to overcome the diffraction limit, which in conventional optics determines the smallest possible lateral dimension for such devices.[1,2] One-dimensional metallic nanostructures such as gold and silver nanowires (NWs) have become attractive candidates as nanoscale optical components because of their ability to act as subwavelength waveguides under visible and near-infrared excitation.[6−22] A nanoscale plasmonic waveguide is realized by coupling light to the collective oscillation of the conduction band electrons, known as surface plasmon polaritons (SPPs).[23] Propagation of SPPs can extend over many micrometers, but is ultimately limited by significant radiative and nonradiative losses by the metal, especially at optical frequencies.[23,24] The NW fabrication method has been found to play an important role for the loss process. Lithographically fabricated NWs[9−12] suffer losses from scattering at the rough surfaces and grain boundaries.[13] In contrast, chemical synthesis of NWs yields highly crystalline structures with smooth surfaces, resulting in significantly lower losses and hence longer propagation lengths.[8,13]

As silver suffers the lowest intrinsic losses among plasmonic materials, SPP propagation characteristics for chemically grown silver NWs have lately been extensively investigated.[14−22,25] Upon excitation at one end of a silver NW, SPP propagation can easily be visualized by the observation of light emission from the opposite end. The SPP is not just converted back into photons at the opposite end but is also reflected and then interferes with itself so that the NW acts as a Fabry−Perot-type resonator.[8,26−28] The output spectrum therefore shows interference fringes, and their amplitude and frequency spacing can be used to determine the SPP propagation length.[8,13,26,27] Another approach to determine the propagation length involves placing multiple or variable input and output couplers like nanoparticle antennas or dielectric waveguides along the NW and monitoring the emission intensity as a function of distance from the input.[14−17,29−31] These studies

* Address correspondence to slink@rice.edu.

Received for review June 19, 2012 and accepted August 19, 2012.

Published online August 19, 2012
10.1021/nn3027112

revealed propagation lengths of more than 10 μm for silver NWs under visible and near-infrared excitation (400−800 nm). SPP propagation in silver NWs has also been studied with interconnected waveguides, where interference and routing of different SPP modes have been demonstrated.[16,18,32,33]

For gold NWs, SPP propagation suffers additional damping due to interband absorption at optical frequencies.[23,24] The direct observation of SPP propagation is therefore more difficult in gold NWs, especially when the waveguide is longer than the SPP propagation length so that no emission from the distal end of the NW can be observed. For this reason, in spite of their superior chemical stability, gold NWs have been deemed less attractive than their silver counterparts for waveguide applications, which is reflected by the relatively few studies on gold NW waveguides. Most studies of SPP propagation in gold waveguides have focused on narrow gold stripes and wires that were fabricated by electron-beam lithography.[9−12] Scanning near-field optical microscopy (SNOM) has been used to map the near-field intensity of the propagating SPP modes.[10−12] These studies revealed moderate propagation lengths of 2−4 μm at visible and near-infrared wavelengths (400−800 nm),[11−13] whereas a long propagation length of ∼10 μm was observed only for excitation in the infrared at 1550 nm.[10] The short propagation length under optical excitation can be attributed to various damping channels that include surface scattering and interband absorption.

Although SNOM is an accurate and convenient imaging method, it is also more complex and expensive than far-field microscopy techniques. However, a direct far-field measurement of propagating SPP modes is not possible, as plasmons are converted into photons only at defects, such as the NW ends, kinks, or nanoparticle antennas, which break the symmetry and allow for direct plasmon−photon conversion.[14−16,29−31] As it is difficult to control the spatial positions of such defects, indirect imaging techniques have been developed to elucidate the SPP propagation in metallic waveguides. A popular approach has been to overcoat the plasmonic NW with a chromophore, which emits after excitation by the SPP near-field.[32,34−36] The emission intensity is proportional to the SPP near-field intensity so that the decay of the emission along the NW yields the propagation length. Irreversible bleaching of the chromophore can complicate the correct extraction of the propagation length, although the use of more photostable quantum dots can circumvent this issue. Our group has recently taken advantage of the photobleaching properties of a fluorescent polymer to instead create permanent maps of the photobleach intensity distribution that can simply be read out with a low-power laser.[37] Using this approach, bleach-imaged plasmon propagation (BIIPP),[37,38] we measured a propagation length smaller than 2 μm for chemically synthesized, short (6 μm), gold NWs at 532 nm.[37] The short propagation length at this wavelength can be ascribed to significant damping of the SPPs close to the interband transition.

Given the limited number of studies on chemically prepared gold NWs, the full potential of such NWs as an optical waveguide has yet to be established. To the best of our knowledge, only a recent study by Pelton and co-workers[36] has depicted SPP propagation in long gold NWs that were prepared by colloidal methods. Using fluorescence imaging, they found propagation lengths of 2.4−3.6 μm for wavelengths in the range of 760−860 nm. They clearly identified the observed SPP as the lowest order $m = 0$ mode. Although they noted that higher order SPP modes should also be supported by these ∼100 nm wide gold NWs, no experimental evidence for such modes was observed. In the present paper, we use BIIPP to characterize SPP propagation at 785 nm in very similar chemically grown 15 μm long and ∼100 nm wide gold NWs. We observe a much longer propagation length, 7.5 ± 2.0 μm. Using electrodynamics simulations, we show that these SPPs are higher order ($m = 1$) SPP modes, whose excitation cross sections are much smaller than the more intense $m = 0$ mode with short propagation length. A comparison with direct fluorescence imaging gives further insight to why our BIIPP measurements are particularly sensitive to these higher order SPP modes and shows the complementarities of BIIPP and fluorescence imaging.

RESULTS AND DISCUSSION

Figure 1 shows a representative BIIPP study carried out on gold NWs at 785 nm for different exposure times. The sample preparation is detailed in the Methods section. In short, a glass coverslip decorated with pentahedrally twinned gold NWs was spin-coated with Cardiogreen (CG) dye to produce a film with a thickness of 4−5 nm, as verified by atomic force microscopy (AFM). Figure 1A shows a sample-scanned fluorescence image of CG coated over a gold NW using an excitation wavelength of 785 nm and a low power of 0.07 μW. The fluorescence over the NW is enhanced due to plasmon−exciton interactions.[39−41] This enhancement depends on the thickness of the dye coating, and by optimizing the dye concentration, a 4−5 times enhancement on the NW compared to the background was achieved. To investigate SPP propagation for a gold NW, one end of the NW was continuously exposed for 10−40 min to a 785 nm laser focused to a diffraction-limited spot size, using an increased laser power of 12−15 μW. Another sample-scanned fluorescence image was then recorded at the original low excitation power (not shown).[37,38] Continuous laser exposure at the NW end leads to the excitation of SPPs that propagate along the NW and induce irreversible

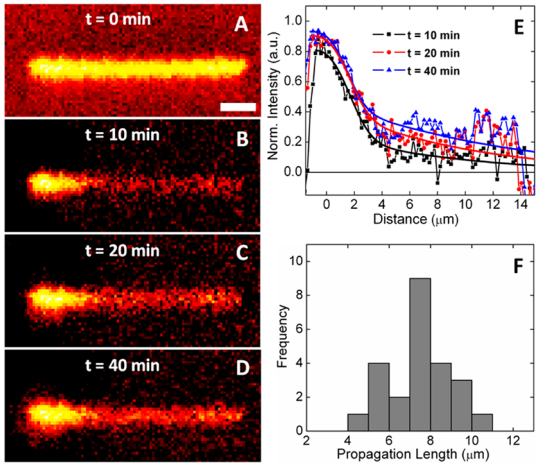

Figure 1. (A) Sample-scanned fluorescence image of a CG-coated gold NW recorded at a low excitation power of 0.07 μW using a 785 nm laser. The scale bar corresponds to 2 μm. (B–D) Difference images obtained by subtracting the images recorded after continuous end excitation with a higher power of 12 μW from the original image (A) for different exposure times of t = 10 min (B), t = 20 min (C), and t = 40 min (D). (E) Width-averaged intensity line sections taken along the long NW axis for the corresponding difference images (B–D). Also shown are fits (lines) using eq 1, which yield a SPP propagation length of L_{BIIPP} = 9.0 ± 1.0 μm, independent of the exposure time. (F) Histogram of propagation lengths measured for 24 individual gold NWs. The average is $\langle L_{BIIPP} \rangle$ = 7.5 ± 2.0 μm.

photobleaching of the CG dye through plasmon–exciton coupling, which is dependent on the intensity of the SPP near-field. By subtracting the second image recorded after CG photobleaching from the initial image we obtained a spatial map of the photobleach intensity, which is directly related to the damping of the SPP. For example, Figure 1B, which shows the difference image after 10 min of laser exposure, illustrates that photobleaching is not confined only to the area of direct laser excitation (left NW end) but extends toward the distal end of the NW. This photobleaching intensity along the NW increases progressively with increasing exposure time, which is evident from the difference images created after 20 min (Figure 1C) and 40 min (Figure 1D) of continuous laser exposure.

From the difference images in Figure 1B–D we obtained a SPP propagation length, L_{BIIPP}, of 9.0 ± 1.0 μm. The width-averaged line sections (Figure 1E), created from the difference images for different exposure times, were fit to eq 1 (Methods section). Equation 1 is based on a kinetic model for the photobleaching, which is caused by two effects: direct laser excitation and an exponentially decaying near-field of the propagating SPP wave. The model assumes that the dye molecules act only as reporters of the local near-field so that the degree of photobleaching at a particular location on the NW is directly proportional to the intensity or the square of the electric field of the SPP. According to this model, the measured propagation length is independent of the exposure time t. The propagation lengths obtained by fitting the line sections in Figure 1E for t = 10 min, t = 20 min, and t = 40 min were indeed the same within the experimental error at L_{BIIPP} = 9.0 ± 1.0 μm. Including the NW shown in Figure 1A–D, we determined the SPP propagation length at 785 nm for a total of 24 gold NWs using BIIPP. Figure 1F shows a histogram of propagation lengths summarizing our measurements. The average propagation length was found to be $\langle L_{BIIPP} \rangle$ = 7.5 ± 2.0 μm. The distribution of propagation lengths was most likely due to variations in the NW width, although other factors such as differences in tip geometry and surface roughness can be significant too.[18,23,37] The excellent agreement with the model (eq 1) and the good reproducibility of the BIIPP measurements validate the long SPP propagation length determined here.

An average propagation length of $\langle L_{BIIPP} \rangle$ = 7.5 ± 2.0 μm for gold NWs at 785 nm is significantly longer than what has been reported before.[11–13,36,37] Previous measurements in the 400–800 nm wavelength region for nanoscale gold waveguides of similar dimensions as used here reported propagation lengths of only 2–4 μm.[11–13,36,37] Among these reports, a recent study by Pelton and co-workers is particularly relevant because similar pentahedrally twinned gold NWs were used and a fluorescence-based imaging technique was employed as well.[36] They used direct fluorescence imaging (DFI) *via* two-photon excitation with a tunable femtosecond laser and determined propagation lengths of 2.4–3.6 μm for an excitation wavelength range of 760–860 nm.[36]

In DFI, the fluorescence of a molecular dye or semiconductor quantum dot, excited by the propagating SPP near-field of plasmonic waveguides, is imaged directly on a CCD camera.[32,34–36] The BIIPP approach, which is basically the inverse of DFI, has the advantage of being able to integrate the SPP-induced near-field for long times and thus amplify weak signals. This difference arises from the fact that, after all the molecules have been bleached by direct laser excitation, the signal at the NW end has reached saturation, while the photobleaching intensity caused by SPP propagation can further increase with exposure time (Figure 1E) without the danger of overexposure and damage to the CCD camera as in DFI. On the other hand, DFI requires only several tens of seconds to a few minutes of exposure time. Thus the techniques are complementary. To understand the long propagation length for gold NWs at 785 nm measured by BIIPP, we therefore performed DFI using the same dye, CG.

A shorter SPP propagation length in agreement with previous studies was indeed obtained when using DFI. A representative example of DFI for a single NW coated with CG is shown in Figure 2A. The fluorescence image was recorded on a CCD camera with an integration time of 1 min under continuous 785 nm laser exposure at one end of the NW. The same microscope setup as in

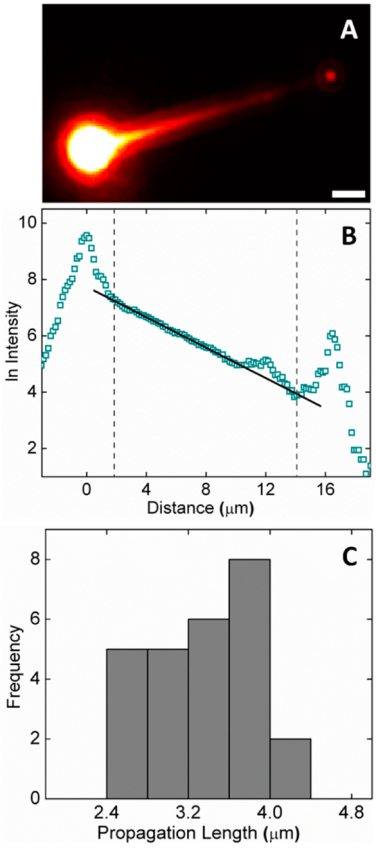

Figure 2. (A) Fluorescence image of SPP propagation with 785 nm laser irradiation at the left end of a single gold NW. The CCD camera integration time was 1 min, and the excitation power was 2.0 μW. The scale bar corresponds to 2 μm. (B) Intensity line section along the long NW axis with the *y*-axis set to a natural log-scale. A fit to the linear portion of the data, highlighted by the dashed lines, gives a propagation length of $L_{DFI} = 3.7 \pm 0.2$ μm. (C) Histogram of propagation lengths measured by DFI for 26 individual NWs. The average propagation length is $\langle L_{DFI} \rangle = 3.5 \pm 0.7$ μm.

BIIPP, apart from the detector, was used, and the only significant difference from the BIIPP measurement was the sample preparation. To optimize the fluorescence contrast between the NW and the background in DFI, a five times lower dye concentration was used, resulting in a significantly thinner dye layer. The intensity line section, when plotted on a semilog scale as shown in Figure 2B, yields an SPP propagation length of $L_{DFI} = 3.7 \pm 0.2$ μm through a linear fit to the data within the appropriate range, excluding the regions of direct laser excitation as well as the distal end, where plasmon–dye coupling is enhanced due to symmetry breaking (Figure 2B). A histogram of 26 NWs measured by DFI revealed a mean SPP propagation length of $\langle L_{DFI} \rangle = 3.5 \pm 0.7$ μm (Figure 2C). This propagation length is similar to the one obtained by Pelton and co-workers[36] despite the fact that they used a different fluorophore, which was excited *via* a two-photon process.

As with BIIPP, a considerable distribution of propagation lengths is seen in DFI. These distributions can largely be attributed to the variations in the NW width based on the results of previous analytical calculations,[36] which showed that the propagation length of the lowest order mode ($m = 0$) increases by 0.5 μm for a 20 nm increase in diameter from 100 to 120 nm of gold NWs excited at 810 nm. Because the experimental variation in NW diameters for our sample was similar, these calculations demonstrate that the measured spread in propagation lengths using DFI ($\langle L_{DFI} \rangle = 3.5 \pm 0.7$ μm) is mainly due to the dispersion of NW diameters. Although the propagation lengths measured with BIIPP were larger, the relative error was comparable ($\langle L_{BIIPP} \rangle = 7.5 \pm 2.0$ μm), which is consistent with the assignment that the experimental distribution was mainly caused by variations in NW diameter.

We next look at possible reasons why the propagation length obtained by BIIPP ($\langle L_{BIIPP} \rangle = 7.5$ μm) for these NWs differs significantly from the value measured by DFI ($\langle L_{DFI} \rangle = 3.5$ μm). Because the difference in the propagation length measured by BIIPP and DFI is roughly a factor of 2, a possible explanation could be that the photobleaching occurs *via* a two-photon process. However, a laser power dependence revealed that both BIIPP and DFI scale linearly with intensity. Another reason for the longer propagation length in BIIPP could be amplification or gain of the SPP by the thicker dye layer on the NWs.[42] Recent studies have shown that an optically pumped dye layer can significantly amplify SPP propagation, where the amplification was manifested by enhanced emission at the output end of the waveguide.[42−45] In the present study, the dye photobleaching in BIIPP has been carried out at quite high excitation powers (12−15 μW) for long exposure times (typically 20 min), and therefore a secondary process such as gain cannot necessarily be ruled out.

To establish if there is a significant contribution from the dye layer acting as a gain medium, we have performed a control experiment, in which we first destroyed part of the dye layer in the middle of the NW and then performed a BIIPP experiment (Figure 3). The dye layer within the region indicated by the dashed lines in Figure 3A was photobleached to create a gap in the fluorescence profile of the NW. The dye molecules in this region could therefore no longer contribute to any possible gain. We then carried out a BIIPP experiment on the same NW, where the image in Figure 3A served as the initial image before photobleaching. After 20 min of continuous laser exposure at the left end of the NW, another fluorescence image was recorded (Figure 3B). The difference image, given in Figure 3C, shows that despite the gap in the middle of the NW, SPP propagation remained unaffected, as evident by the strong photobleaching to the right of the gap (compare Figures 1C and 3C). We hence conclude that gain due to the dye is not responsible for the observed long propagation length. This conclusion is also consistent with the fact that the propagation

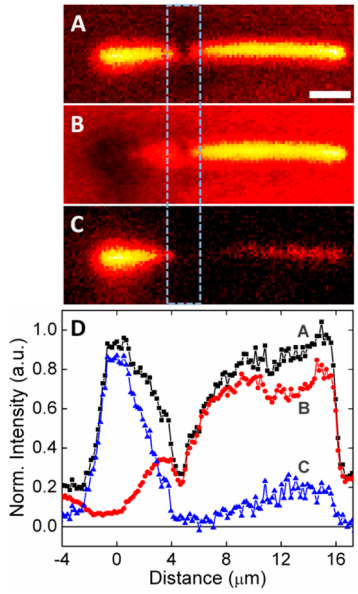

Figure 3. (A) Sample-scanned fluorescence image of a CG-coated gold NW with a gap in the dye fluorescence response near the middle of the NW, created by direct laser photobleaching with 12 μW of power for 2 min. The scale bar corresponds to 2 μm. (B) Fluorescence image taken after excitation of the same NW at the left end with 20 μW of 785 nm laser light for 20 min. The laser power for the image acquisition was 0.07 μW for (A) and (B). (C) Difference image obtained by subtracting (B) from (A). (D) Width-averaged line sections for the corresponding images in (A–C). SPP propagation beyond the gap, highlighted by the dashed lines in (C), is clearly observable in both the difference image (C) and the corresponding line section (D).

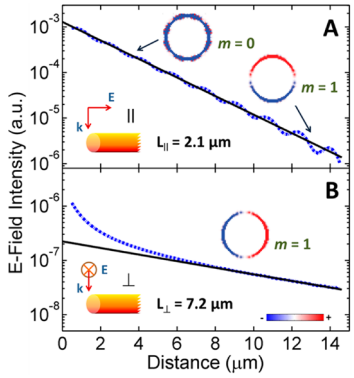

Figure 4. FDTD simulations of SPP propagation (blue curves) for a 15 μm long NW with a diameter of 100 nm for 785 nm plane wave illumination at the left NW end. The excitation polarization was parallel (A) and perpendicular (B) with respect to the long axis of the NW. The propagating SPP modes were identified on the basis of their surface charge distribution, and the cross-sectional views of the surface charges are shown as insets. Under parallel polarized excitation (A), the m = 0 mode dominates over the much weaker m = 1 mode. The latter is visible only further along the NW. Under perpendicular polarized excitation (B), only the m = 1 mode is seen. Appropriate fits (black lines) to the corresponding data yield propagation lengths of $L_{\parallel}$ = 2.1 μm (A) and $L_{\perp}$ = 7.2 μm (B). In (B), the departure of the data from linearity at short distances is due to artifacts associated with modeling the coupling of light into the NW.

length remains constant as a function of exposure time (Figure 1) instead of decreasing with time as more dye molecules are photobleached.

We performed finite difference time domain (FDTD) simulations to gain further insight into the different SPP modes supported in these gold NWs for 785 nm excitation (Figure 4). The dispersion relations and propagation lengths for plasmons in infinite cylindrical nanowires surrounded by concentric shells can be calculated analytically as well.[46–48] However, the solutions that involve cylindrical harmonics cannot be expressed in closed form.[47,48] We therefore chose to model the system using the FDTD method and proceeded as follows: the NW was placed in a continuous dielectric medium with the same permittivity as glass (the value for the dye is similar to glass), and the NW was excited at one end with a plane wave with a wavelength of 785 nm. Figure 4A and B show the electric field intensities along the NW for excitation polarized parallel (4A) and perpendicular (4B) to the long NW axis. The propagation length strongly depends on the excitation polarization as it varies from $L_{\parallel}$ = 2.1 μm for parallel excitation to $L_{\perp}$ = 7.2 μm for perpendicular excitation. On the basis of the surface charge plots (insets of Figure 4), we can assign different SPP modes to these propagation lengths. Under parallel excitation, the dominant mode is m = 0 with only a small contribution from m = 1 (Figure 4A), while for perpendicular excitation only the m = 1 mode is visible (Figure 4B). Therefore, we can conclude that the m = 0 mode has a shorter propagation length of L = 2.1 μm and the m = 1 mode has a longer propagation length of L = 7.2 μm. In addition, it is important to note that the m = 0 mode was much more efficiently excited, by a factor of about 1000 times, compared to the m = 1 mode. Interestingly, the simulated propagation lengths of $L_{\perp}$ = 7.2 μm and $L_{\parallel}$ = 2.1 μm closely resemble the values obtained by experiments, L_{BIIPP} = 7.5 μm and L_{DFI} = 3.5 μm. Because the experiments presented so far have been carried out with circularly polarized light, a polarization dependence of BIIPP and DFI was performed to investigate if different modes were excited by these two techniques.

The propagation lengths are surprisingly insensitive to the excitation polarization for both BIIPP and DFI (Figure 5). Figure 5A and B show difference images recorded for 785 nm excitation with polarization parallel and perpendicular to the long NW axis, respectively. The width-averaged line sections created from 5A and 5B as well as the fits (Figure 5C) reveal that the propagation lengths are comparable for these two measurements and furthermore agree well with the distribution of values measured for circular polarized excitation (Figure 1F). However, parallel polarized excitation leads to more efficient bleaching for the same exposure time of 20 min, suggesting that the in-coupling efficiency is larger for that excitation polarization. Although we had to perform these BLIPP

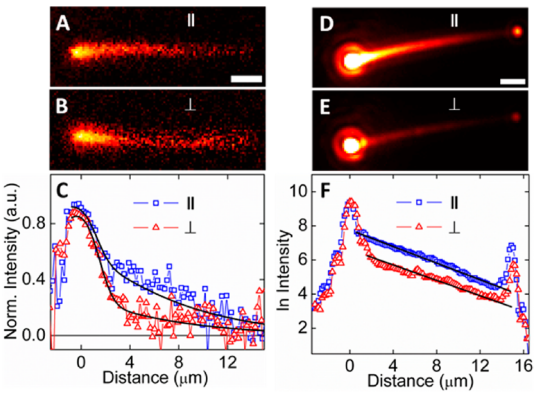

Figure 5. Excitation polarization dependence of BIIPP (A–C) and DFI (D–F). BIIPP: Difference images for excitation polarization parallel (A) and perpendicular (B) to the long axis of a gold NW taken with a scan power of 0.07 μW and a bleaching power of 12 μW for an exposure time of 20 min. (C) Corresponding width-averaged line sections with fits: $L_{\parallel}$ = 7.6 μm and $L_{\perp}$ = 6.8 μm. DFI: Fluorescence images recorded under parallel (D) and perpendicular (E) polarized excitation using a laser power of 2.0 μW and an integration time of 1 min. (F) Corresponding line sections with linear fits on a natural log intensity scale: $L_{\parallel}$ = 4.0 μm, $L_{\perp}$ = 4.3 μm. The scale bars correspond to 2 μm.

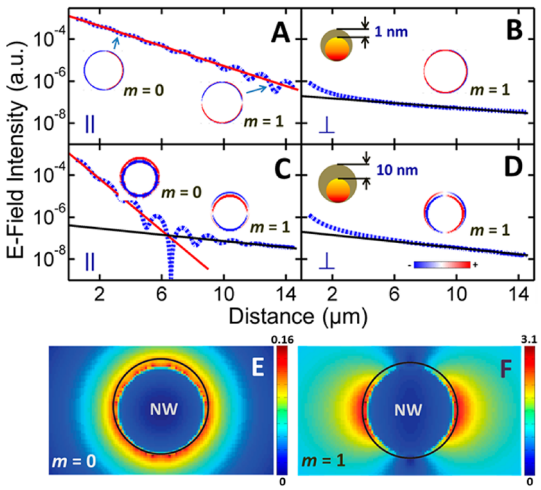

Figure 6. Dependence of SPP propagation on the thickness of the dye layer, modeled as a lossy medium. FDTD simulations of SPP propagation (blue curves) for a 15 μm long NW with a diameter of 100 nm for 785 nm plane wave illumination at the left NW end are shown using excitation polarization parallel (A, C) and perpendicular (B, D) with respect to the long axis of the NW. The NW was placed on top of a glass substrate and covered by an absorptive dye layer, as illustrated by the schematic inset. Simulations were performed as a function of thickness d of this dye layer. Two extreme cases are illustrated here: (A, B) d = 1 nm (thin layer) and (C, D) d = 10 nm (thick layer). Cross-sectional views of the surface charge distributions are shown as insets to identify the m = 0 and m = 1 modes. Propagation lengths corresponding to these different modes were obtained from the respective fits (lines). For the thin layer (A, B), the propagation lengths are $L_{\parallel}$ = 1.8 μm (A) and $L_{\perp}$ = 7.0 μm (B), corresponding to the m = 0 and m = 1 modes, respectively. For the thick layer (C, D), parallel polarization (C) excites m = 0 and m = 1 modes, which can now be clearly distinguished from each other and allows us to determine two propagation lengths of $L_{\parallel}$ = 0.7 μm for the m = 0 mode and $L_{\parallel}$ = 5.8 μm for the m = 1 mode. Under perpendicular polarized excitation (D) only the m = 1 mode is supported, with a propagation length of $L_{\perp}$ = 5.7 μm. (E, F) Contour plots of the spatial distribution of the E-field strengths for the m = 0 mode (E) and m = 1 mode (F). The black circle indicates the upper boundary of the dye layer. Note that within that boundary the E-field is much stronger for the m = 0 mode compared to the m = 1 mode.

experiments on different NWs, we repeated these measurements seven times and always observed the same trend. The corresponding DFI experiment is illustrated in Figure 5D–F, which show fluorescence images for the same gold NW excited with parallel (5D) and perpendicular (5E) polarized 785 nm light. The line sections and fits again yield similar propagation lengths, which are also consistent with the distribution shown in Figure 2C. As in the case of BIIPP, a drop in intensity is found in DFI for perpendicular polarized excitation light and is similarly attributed to a difference in coupling efficiency. The weak polarization dependence of both techniques can be rationalized by considering the fact that the tip geometry is idealized in the simulations compared to the experiment. As shown previously,[18] irregular tip geometries in real NWs can easily mix different polarizations, which explains the observed insensitivity toward the excitation polarization. The polarization dependence is therefore not capable of explaining the different propagation length measured with BIIPP and DFI.

It has been shown recently that the substrate plays an important role for SPP propagation in NWs as coupling to absorbing compared to dielectric substrates can severely dampen the propagation length.[49] Although the substrate is glass for both BIIPP and DFI, the major difference in the experimental conditions between BIIPP and DFI was the thickness of the dye coating on the NWs. The dye layer was appreciably thinner in DFI than the one in the BIIPP measurements (4–5 nm), because the solution used for spin-coating was diluted by a factor of 5 for DFI. We estimate the resulting dye thickness to be around 1 nm. Different dye layer thicknesses were used to optimize the contrast for both measurements independently. However, we tested DFI with a sample prepared for BIIPP, but were unable to observe a fluorescence signal, presumably due to self-quenching of the thicker dye layer. We also investigated the opposite, BIIPP with a thin dye layer. Intermediate dye concentrations were also prepared and studied by BIIPP and DFI, but we were not able to find a suitable compromise to study the same NW first by DFI and then by BIIPP. Therefore, we turn again to FDTD simulations.

We now model the dye layer as a lossy medium and find that depending on the thickness the m = 0 and m = 1 modes identified before are affected differently. The results of these FDTD simulations are given in Figure 6. Figure 6A and B show the simulated electric field intensities *vs* distance along the NW for a 1 nm thin dye layer using an excitation polarization

parallel and perpendicular to the NW axis, respectively. Figure 6C and D show the corresponding results for a 10 nm thick dye layer. Although this thickness is significantly larger than the experimental thickness determined for the BIIPP samples, we chose this case to better understand the effect of an absorbing medium like a film of dye molecules. Instead of acting as a dielectric with a certain refractive index, the dye molecules were now assumed to form a partially conductive medium with a complex dielectric constant that induces absorptive damping of propagating SPPs. When the dye layer is thin (Figure 6A and B), the results resemble those already presented in Figure 4 for the case when the dye just acts as a passive dielectric medium. The propagation lengths as well as the relative amplitudes of both $m = 0$ and $m = 1$ modes are similar with and without the lossy dye layer for both parallel and perpendicular excitation polarizations. A thin dye layer hence has little effect on the measured SPP propagation characteristics.

However, when the thickness of the lossy dye layer was increased to 10 nm (Figure 6C and D), a pronounced difference is observed in the simulated propagation lengths. For parallel polarized excitation (Figure 6C), the $m = 1$ mode is no longer buried under the more intense $m = 0$ mode because the latter is strongly dampened by the thicker absorbing dye layer. This quenching of the $m = 0$ mode is particularly obvious in the propagation length, which is reduced to $L_{\parallel} = 0.7\ \mu$m from 2.1 μm without the lossy dye layer (Figure 4A). In contrast, the effect of the thicker dye layer on the $m = 1$ mode is relatively weak. The propagation length is only slightly reduced for this mode ($L_{\parallel} = 5.8\ \mu$m and $L_{\perp} = 5.7\ \mu$m, compared to $L_{\perp} = 7.2\ \mu$m without the dye layer, as shown in Figure 4B). The reason for a greater quenching of the $m = 0$ mode compared to the $m = 1$ mode can be understood from the comparison of the spatial distribution of the E-field strengths shown in Figure 6E and F. Within the boundary of the lossy medium, as indicated by the black circle, the $m = 0$ mode has a much stronger E-field confined in a shorter distance from the surface of the NW than the $m = 1$ mode. The greater overlap of the $m = 0$ mode with the dye medium therefore allows for better coupling and larger absorptive losses, consistent with the stronger quenching of the $m = 0$ mode.

The FDTD simulations in Figure 6 explain the differences observed in the BIIPP and DFI measurements. For DFI, the dye layer is thin and does not significantly perturb the dominant $m = 0$ mode, which is the one that is observed experimentally because its excitation cross section is a factor of 1000 larger compared to the $m = 1$ mode. The latter therefore is not registered in the experiment especially because the integration time has to be kept short in order not to saturate the CCD camera. The measured propagation length $\langle L_{DFI} \rangle = 3.5 \pm 0.7\ \mu$m agrees with the calculated value of $L_{\parallel} = 2.1\ \mu$m. For BIIPP, the dye layer is much thicker and effectively dampens the $m = 0$ mode. The propagation length of this mode is now so short (<1 μm) that it is masked by the beam width of the incident laser. Therefore only the $m = 1$ mode with the longer propagation length is observed in the BIIPP measurements. The measured propagation length $\langle L_{BIIPP} \rangle = 7.5 \pm 2.0\ \mu$m agrees with the calculated values of $L_{\parallel} = 5.8\ \mu$m and $L_{\perp} = 5.7\ \mu$m.

CONCLUSIONS

We have measured SPP propagation in long gold NWs at 785 nm using BIIPP, a technique where the photobleaching of a dye due to coupling to the plasmonic near-field is monitored and then related to SPP propagation. Our results are compared with DFI, an approach that is based on the direct imaging of the fluorescence from dye molecules on top of the NWs to visualize the propagating SPP modes. A substantially longer propagation length is revealed in BIIPP. Control experiments ruled out amplification of SPP propagation by the dye medium. Detailed FDTD simulations show that the results from the two approaches are consistent and that two different SPP modes are excited when light is focused on a NW end: an intense $m = 0$ mode with short propagation length and a weaker $m = 1$ mode with longer propagation length. The propagation length of the $m = 0$ mode is found to be drastically reduced by the presence of a thick absorbing dye medium around the NW, while the $m = 1$ mode is much less sensitive. In the DFI approach, where a thin dye coating is used, only the more intense $m = 0$ mode can be resolved. In contrast, in the BIIPP approach, where a thick coating is used, the contribution from the $m = 0$ mode is quenched and the propagation of the $m = 1$ can be resolved. Our results thus demonstrate the complementarities of the DFI and BIIPP approaches and confirm the existence of a higher order mode with long propagation length in gold NWs. Most importantly we show that the propagation lengths of different SPP modes can be controlled independently by coating NWs with absorbing dyes that can serve as mode-specific dampers.

METHODS

Sample Preparation. Gold NWs stabilized by cetyltrimethylammonium bromide (CTAB) were synthesized by tip selective growth of purified pentahedrally twinned gold nanorods. The latter were synthesized by a procedure as described elsewhere.[50,51] The resulting NWs were crystalline with highly uniform surfaces. They were 12−15 μm long with an average diameter of 90 ± 10 nm. Glass coverslips were cleaned by sonicating them in milli-Q water and acetone and then by exposing them to oxygen plasma (Harrick Plasma Cleaner) for

1 min after drying. NWs were deposited on the coverslips by dropcasting 10 μL of the appropriately diluted colloidal solution. In order to remove excess CTAB, the coverslips were then washed with warm ethanol (30−40 mL) and dried under a low flow of nitrogen. Then, a layer of the dye Cardiogreen (Sigma) was spin-coated (Headway Research Inc.) onto the sample at 6000 rpm for 40 s. For BIIPP, the concentration of the dye solution was 0.5 mg/mL (6.5×10^{-4} mol L^{-1}). For DFI, the dye concentration was 5 times lower, 0.1 mg/mL (1.3×10^{-4} mol L^{-1}). The average thickness of the dye layer for the BIIPP experiments was determined by AFM (Veeco) to be around 4−5 nm. The dye layer for the DFI measurements was too thin to be measured accurately, but we estimate a thickness of about 1 nm, consistent with the difference in dye concentrations.

BIIPP Measurement. BIIPP measurements were performed by first recording a sample-scanned fluorescence image of a NW using an inverted microscope setup (Axiovert 200) equipped with a piezoelectric scanning stage (Physik Instrumente) that was connected to a surface probe controller (RHK Technology). Laser light from a 785 nm diode laser (Power Technology Inc.) was focused onto the sample through a 50× Zeiss air-spaced objective with a numerical aperture of 0.8. The fluorescence was collected by the same objective using appropriate dichroic and notch filters and directed to an avalanche photodiode detector (Perkin-Elmer). The resolution for 785 nm excitation, determined by recording scattering images of 25 × 86 nm gold nanorods, was around 350 nm (fwhm). Typically, sample-scanned fluorescence images were taken of 20 × 20 μm or 25 × 25 μm areas with an integration time of 10 ms/pixel and a resolution of 128 × 128 pixels at a low excitation power of 0.07 μW.

The detailed method of image acquisition and analysis for BIIPP has been documented in previous reports.[37,38] In brief, after the first image was acquired, the laser was focused onto one end of the NW, the laser power was then increased to typically 12−15 μW, and the sample was irradiated for usually a few tens of minutes. During this exposure, light from the laser launched SPPs along the NW waveguide and the near-field of the propagating SPPs interacted with the dye molecules, causing them to photobleach irreversibly over time. Then, the laser power was reduced to the initial value and a second fluorescence image of the same region was acquired. A difference image was created by subtracting the second image after photobleaching from the first image before photobleaching using a MATLAB (v. R2010b) program. The difference image therefore represents the amount of photobleaching due to direct laser excitation at one NW end and SPP propagation along the NW. To account for small sample and focus drift during the exposure period, we performed an image shift correction and background scalar correction before creating the difference image. From the difference image we then created a width-averaged intensity line section along the long NW axis.

The SPP propagation length was determined by fitting the width-averaged line sections to a kinetic model[37] that considered the dye photobleaching as a first-order reaction with excitation from two sources: direct laser excitation, modeled as a Gaussian intensity profile, and the SPP near-field, which decays exponentially along the NW. This model leads to the following equation describing the photobleach intensity I_{bleach} as a function of position x and time t:[37]

$$I_{bleach} = 1 - \exp(-kI_{G,0}\,t\,\exp(-x^2/2\sigma^2) - kI_{SPP,0}\,t\,\exp(-x/L)) \quad (1)$$

where $kI_{G,0}$ and $kI_{SPP,0}$ are the products of the dye photobleaching rate constant k and the incident intensities due to Gaussian laser excitation and the SPP near-field at $x = 0$ and were used as variable fit parameters. σ describe the width of the Gaussian laser beam and was determined from bleaching of the CG dye in an area without NWs. A fit of the width-averaged line section to the above equation yields the SPP propagation length L.

DFI Measurement. For DFI the same microscope setup was used, but a CCD camera (Princeton Instruments) was employed as the detector. Upon continuous laser irradiation at one end of a NW, the CCD camera captured fluorescence images from the entire NW for an integration time of typically 1 min. A background-corrected width-averaged fluorescence intensity line section was extracted from the fluorescence image using a similar procedure to that described above. The fluorescence intensity was plotted on a semilog (natural log) scale, and the linear region was fitted to a line giving the propagation length.

FDTD Simulation. Electromagnetic simulations were carried out using the FDTD method. For the case of a "nonlossy" dye, the gold NWs were modeled as round cylinders with flat ends positioned in an infinite dielectric background with a refractive index of $n = 1.5$. The dimensions of the NW were 15 μm by 100 nm. For the dielectric function of gold, the tabulated values by Johnson and Christy were used.[52] For the case of a "lossy" dye, a cylindrical coating was modeled as shown in the insets of Figure 6. The complex refractive index of the coating was $n = 1.54 + 0.36i$, which was based on assuming an oscillator strength for the optical absorption of the dye of 0.1. The NW and the lossy dye were placed in an infinite dielectric background with a real refractive index of $n = 1.5$. Excitation was carried out with plane waves incident on one end of the NW. No significant differences were observed if a Gaussian beam was used instead of a plane wave. SPP propagation lengths for the different modes were determined from linear fits to semilog plots of the electric field intensity *vs* distance.

Conflict of Interest: The authors declare no competing financial interest.

Acknowledgment. This work was funded by the Robert A. Welch Foundation (C-1664, C-1222), the Office of Naval Research (N00014-10-1-0989), and NSF (CHE-0955286). D.S. was supported by an NSF Graduate Research Fellowship grant (no. 0940902). E.R.Z. acknowledges the financial support by NSF (DMR-1105878).

REFERENCES AND NOTES

1. Gramotnev, D. K.; Bozhevolnyi, S. I. Plasmonics Beyond the Diffraction Limit. *Nat. Photonics* **2010**, *4*, 83–91.
2. Ozbay, E. Plasmonics: Merging Photonics and Electronics at Nanoscale Dimensions. *Science* **2006**, *311*, 189–193.
3. Barnes, W. L.; Dereux, A.; Ebbesen, T. W. Surface Plasmon Subwavelength Optics. *Nature* **2003**, *424*, 824–830.
4. Chang, W.-S.; Slaughter, L. S.; Khanal, B. P.; Manna, P.; Zubarev, E. R.; Link, S. One-Dimensional Coupling of Gold Nanoparticle Plasmons in Self-Assembled Ring Superstructures. *Nano Lett.* **2009**, *9*, 1152–1157.
5. Large, N.; Saviot, L.; Margueritat, J. r. m.; Gonzalo, J.; Afonso, C. N.; Arbouet, A.; Langot, P.; Mlayah, A.; Aizpurua, J. Acousto-Plasmonic Hot Spots in Metallic Nano-Objects. *Nano Lett.* **2009**, *9*, 3732–3738.
6. Nah, S.; Li, L.; Liu, R.; Hao, J.; Lee, S. B.; Fourkas, J. T. Metal-Enhanced Multiphoton Absorption Polymerization with Gold Nanowires. *J. Phys. Chem. C* **2010**, *114*, 7774–7779.
7. Dickson, R. M.; Lyon, L. A. Unidirectional Plasmon Propagation in Metallic Nanowires. *J. Phys. Chem. B* **2000**, *104*, 6095–6098.
8. Ditlbacher, H.; Hohenau, A.; Wagner, D.; Kreibig, U.; Rogers, M.; Hofer, F.; Aussenegg, F. R.; Krenn, J. R. Silver Nanowires as Surface Plasmon Resonators. *Phys. Rev. Lett.* **2005**, *95*, 257403.
9. Krenn, J. R.; Weeber, J. C. Surface Plasmon Polaritons in Metal Stripes and Wires. *Philos. Trans. R. Soc. London Ser. A: Math. Phys. Eng. Sci.* **2004**, *362*, 739–756.
10. Verhagen, E.; Spasenovic, M.; Polman, A.; Kuipers, L. Nanowire Plasmon Excitation by Adiabatic Mode Transformation. *Phys. Rev. Lett.* **2009**, *102*, 203904.
11. Krenn, J. R.; Lamprecht, B.; Ditlbacher, H.; Schider, G.; Salerno, M.; Leitner, A.; Aussenegg, F. R. Non-diffraction-limited Light Transport by Gold Nanowires. *Europhys. Lett.* **2002**, *60*, 663–669.
12. Dallapiccola, R.; Dubois, C.; Gopinath, A.; Stellacci, F.; Dal Negro, L. Near-field Excitation and Near-field Detection of Propagating Surface Plasmon Polaritons on Au Waveguide Structures. *Appl. Phys. Lett.* **2009**, *94*, 243118.

13. Kusar, P.; Gruber, C.; Hohenau, A.; Krenn, J. R. Measurement and Reduction of Damping in Plasmonic Nanowires. *Nano Lett.* **2012**, *12*, 661–665.
14. Sanders, A. W.; Routenberg, D. A.; Wiley, B. J.; Xia, Y. N.; Dufresne, E. R.; Reed, M. A. Observation of Plasmon Propagation, Redirection, and Fan-out in Silver Nanowires. *Nano Lett.* **2006**, *6*, 1822–1826.
15. Knight, M. W.; Grady, N. K.; Bardhan, R.; Hao, F.; Nordlander, P.; Halas, N. J. Nanoparticle-Mediated Coupling of Light into a Nanowire. *Nano Lett.* **2007**, *7*, 2346–2350.
16. Yan, R. X.; Pausauskie, P.; Huang, J. X.; Yang, P. D. Direct Photonic-Plasmonic Coupling and Routing in Single Nanowires. *Proc. Natl. Acad. Sci. U. S. A.* **2009**, *106*, 21045–21050.
17. Akimov, A. V.; Mukherjee, A.; Yu, C. L.; Chang, D. E.; Zibrov, A. S.; Hemmer, P. R.; Park, H.; Lukin, M. D. Generation of Single Optical Plasmons in Metallic Nanowires Coupled to Quantum Dots. *Nature* **2007**, *450*, 402–406.
18. Li, Z. P.; Bao, K.; Fang, Y. R.; Huang, Y. Z.; Nordlander, P.; Xu, H. X. Correlation Between Incident and Emission Polarization in Nanowire Surface Plasmon Waveguides. *Nano Lett.* **2010**, *10*, 1831–1835.
19. Staleva, H.; Skrabalak, S. E.; Carey, C. R.; Kosel, T.; Xia, Y. N.; Hartland, G. V. Coupling to Light, and Transport and Dissipation of Energy in Silver Nanowires. *Phys. Chem. Chem. Phys.* **2009**, *11*, 5889–5896.
20. Li, Z. P.; Hao, F.; Huang, Y. Z.; Fang, Y. R.; Nordlander, P.; Xu, H. X. Directional Light Emission from Propagating Surface Plasmons of Silver Nanowires. *Nano Lett.* **2009**, *9*, 4383–4386.
21. Song, M. X.; Bouhelier, A.; Bramant, P.; Sharma, J.; Dujardin, E.; Zhang, D. G.; Colas-des-Francs, G. Imaging Symmetry-Selected Corner Plasmon Modes in Penta-Twinned Crystalline Ag Nanowires. *ACS Nano* **2011**, *5*, 5874–5880.
22. Shegai, T.; Miljkovic, V. D.; Bao, K.; Xu, H. X.; Nordlander, P.; Johansson, P.; Kall, M. Unidirectional Broadband Light Emission from Supported Plasmonic Nanowires. *Nano Lett.* **2011**, *11*, 706–711.
23. Raether, H. *Surface Plasmons on Smooth and Rough Surfaces and on Gratings*; Springer: New York, 1988.
24. Boltasseva, A.; Atwater, H. A. Low-Loss Plasmonic Metamaterials. *Science* **2011**, *331*, 290–291.
25. Wang, W. H.; Yang, Q.; Fan, F. R.; Xu, H. X.; Wang, Z. L. Light Propagation in Curved Silver Nanowire Plasmonic Waveguides. *Nano Lett.* **2011**, *11*, 1603–1608.
26. Allione, M.; Temnov, V. V.; Fedutik, Y.; Woggon, U.; Artemyev, M. V. Surface Plasmon Mediated Interference Phenomena in Low-Q Silver Nanowire Cavities. *Nano Lett.* **2008**, *8*, 31–35.
27. Dorfmuller, J.; Vogelgesang, R.; Weitz, R. T.; Rockstuhl, C.; Etrich, C.; Pertsch, T.; Lederer, F.; Kern, K. Fabry-Perot Resonances in One-Dimensional Plasmonic Nanostructures. *Nano Lett.* **2009**, *9*, 2372–2377.
28. Wiley, B. J.; Lipomi, D. J.; Bao, J. M.; Capasso, F.; Whitesides, G. M. Fabrication of Surface Plasmon Resonators by Nanoskiving Single-Crystalline Gold Microplates. *Nano Lett.* **2008**, *8*, 3023–3028.
29. Wang, L. L.; Zou, C. L.; Ren, X. F.; Liu, A. P.; Lv, L.; Cai, Y. J.; Sun, F. W.; Guo, G. C.; Guo, G. P. Exciton-Plasmon-Photon Conversion in Silver Nanowire: Polarization Dependence. *Appl. Phys. Lett.* **2011**, *99*, 061103.
30. Hutchison, J. A.; Centeno, S. P.; Odaka, H.; Fukumura, H.; Hofkens, J.; Uji-i, H. Subdiffraction Limited, Remote Excitation of Surface Enhanced Raman Scattering. *Nano Lett.* **2009**, *9*, 995–1001.
31. Fedutik, Y.; Temnov, V. V.; Schops, O.; Woggon, U.; Artemyev, M. V. Exciton-Plasmon-Photon Conversion in Plasmonic Nanostructures. *Phys. Rev. Lett.* **2007**, *99*, 136802.
32. Wei, H.; Li, Z. P.; Tian, X. R.; Wang, Z. X.; Cong, F. Z.; Liu, N.; Zhang, S. P.; Nordlander, P.; Halas, N. J.; Xu, H. X. Quantum Dot-Based Local Field Imaging Reveals Plasmon-Based Interferometric Logic in Silver Nanowire Networks. *Nano Lett.* **2011**, *11*, 471–475.
33. Fang, Y. R.; Li, Z. P.; Huang, Y. Z.; Zhang, S. P.; Nordlander, P.; Halas, N. J.; Xu, H. X. Branched Silver Nanowires as Controllable Plasmon Routers. *Nano Lett.* **2010**, *10*, 1950–1954.
34. Ditlbacher, H.; Krenn, J. R.; Felidj, N.; Lamprecht, B.; Schider, G.; Salerno, M.; Leitner, A.; Aussenegg, F. R. Fluorescence Imaging of Surface Plasmon Fields. *Appl. Phys. Lett.* **2002**, *80*, 404–406.
35. Graff, A.; Wagner, D.; Ditlbacher, H.; Kreibig, U. Silver Nanowires. *Eur. Phys. J. D* **2005**, *34*, 263–269.
36. Wild, B.; Cao, L.; Sun, Y.; Khanal, B. P.; Zubarev, E. R.; Gray, S. K.; Scherer, N. F.; Pelton, M. Propagation Lengths and Group Velocities of Plasmons in Chemically Synthesized Gold and Silver Nanowires. *ACS Nano* **2012**, *6*, 472–482.
37. Solis, D.; Chang, W.-S.; Khanal, B. P.; Bao, K.; Nordlander, P.; Zubarev, E. R.; Link, S. Bleach-Imaged Plasmon Propagation (BIIPP) in Single Gold Nanowires. *Nano Lett.* **2010**, *10*, 3482–3485.
38. Solis, D.; Willingham, B.; Nauert, S. L.; Slaughter, L. S.; Olson, J.; Swanglap, P.; Paul, A.; Chang, W.-S.; Link, S. Electromagnetic Energy Transport in Nanoparticle Chains via Dark Plasmon Modes. *Nano Lett.* **2012**, *12*, 1349–1353.
39. Anger, P.; Bharadwaj, P.; Novotny, L. Enhancement and Quenching of Single-Molecule Fluorescence. *Phys. Rev. Lett.* **2006**, *96*, 113002.
40. Chen, Y.; Munechika, K.; Ginger, D. S. Dependence of Fluorescence Intensity on The Spectral Overlap Between Fluorophores and Plasmon Resonant Single Silver Nanoparticles. *Nano Lett.* **2007**, *7*, 690–696.
41. Kinkhabwala, A.; Yu, Z. F.; Fan, S. H.; Avlasevich, Y.; Mullen, K.; Moerner, W. E. Large Single-Molecule Fluorescence Enhancements Produced by a Bowtie Nanoantenna. *Nat. Photonics* **2009**, *3*, 654–657.
42. De Leon, I.; Berini, P. Amplification of Long-Range Surface Plasmons by a Dipolar Gain Medium. *Nat. Photonics* **2010**, *4*, 382–387.
43. Noginov, M. A.; Podolskiy, V. A.; Zhu, G.; Mayy, M.; Bahoura, M.; Adegoke, J. A.; Ritzo, B. A.; Reynolds, K. Compensation of Loss in Propagating Surface Plasmon Polariton by Gain in Adjacent Dielectric Medium. *Opt. Express* **2008**, *16*, 1385–1392.
44. Noginov, M. A.; Zhu, G.; Mayy, M.; Ritzo, B. A.; Noginova, N.; Podolskiy, V. A. Stimulated Emission of Surface Plasmon Polaritons. *Phys. Rev. Lett.* **2008**, *101*, 226806.
45. Gather, M. C.; Meerholz, K.; Danz, N.; Leosson, K. Net Optical Gain in a Plasmonic Waveguide Embedded in a Fluorescent Polymer. *Nat. Photonics* **2010**, *4*, 457–461.
46. Pritz, J.; Woods, L. M. Surface Plasmon Polaritons in Concentric Cylindrical Structures. *Solid State Commun.* **2008**, *146*, 345–350.
47. Chang, D. E.; Sorensen, A. S.; Hemmer, P. R.; Lukin, M. D. Strong Coupling of Single Emitters to Surface Plasmons. *Phys. Rev. B* **2007**, *76*, 035420.
48. Novotny, L.; Hafner, C. Light Propagation in a Cylindrical Waveguide with a Complex, Metallic, Dielectric Function. *Phys. Rev. E* **1994**, *50*, 4094–4106.
49. Li, Z. P.; Bao, K.; Fang, Y. R.; Guan, Z. Q.; Halas, N. J.; Nordlander, P.; Xu, H. X. Effect of a Proximal Substrate on Plasmon Propagation in Silver Nanowires. *Phys. Rev. B* **2010**, *82*, 241402.
50. Khanal, B. P.; Zubarev, E. R. Purification of High Aspect Ratio Gold Nanorods: Complete Removal of Platelets. *J. Am. Chem. Soc.* **2008**, *130*, 12634–12635.
51. Critchley, K.; Khanal, B. P.; Górzny, M. Ł.; Vigderman, L.; Evans, S. D.; Zubarev, E. R.; Kotov, N. A. Near-Bulk Conductivity of Gold Nanowires as Nanoscale Interconnects and the Role of Atomically Smooth Interface. *Adv. Mater.* **2010**, *22*, 2338–2342.
52. Johnson, P. B.; Christy, R. W. Optical Constants of the Noble Metals. *Phys. Rev. B* **1972**, *6*, 4370–4379.